Transcriptional Fidelity of Mitochondrial RNA Polymerase RpoTm from *Arabidopsis thaliana*

Amit Kumar Yadav †, **Pankaj Kumar Sahoo** †, **Hemant Nath Goswami and Deepti Jain**

Transcription Regulation Lab, *Regional Centre for Biotechnology, NCR Biotech Science Cluster, 3rd Milestone, Faridabad, 121001, India*

Correspondence to Deepti Jain: *deepti@rcb.res.in.*
https://doi.org/10.1016/j.jmb.2019.08.022
Edited by Konstantin Severinov

Abstract

Fidelity of RNA synthesis is essential for the faithful transfer of information from DNA to RNA. A comprehensive analysis of the nucleotide selectivity by the mitochondrial RNA polymerase (RNAP) RpoTm, from *Arabidopsis thaliana,* has been carried out. The kinetic parameters for the incorporation of cognate, noncognate, and oxidized bases have been determined. The results establish high fidelity of mitochondrial transcription resembling those of replicative polymerases in the absence of repair. In addition, RpoTm incorporates oxidized nucleotides with similar efficiency compared with mismatches and is capable of extending the RNA beyond the insertion of the oxidized base. Furthermore, lesion bypass study on RpoTm demonstrates that the enzyme bypasses 8-oxo-guanine by insertion of adenine leading to C to A mutations in RNA. Homology modeling of RpoTm elongation complex allows delineation of the residues necessary for stabilizing the incoming NTP substrate and for posing the template nucleotide residue. Substitution of these residues leads to compromise in the activity of the enzyme corroborating their importance in RNA synthesis. Comparison of the data with T7 RNAPs indicates that low efficiency of misincorporation is a universal strategy used by single-subunit RNAPs for maintaining high fidelity in the absence of proofreading and repair activity in mitochondria.

Introduction

Transcription is central to the process of expression of genetic material in the cell. Transcriptional fidelity is essential to preserve the integrity of the genetic code and overall health of the organism [1]. Transcriptional errors result in the production of erroneous mRNAs which in turn can result in translational and splicing defects and shortened lifespan of an organism [2,3]. Transcriptional errors can be transient or can lead to a heritable phenotype causing growth defects and diseases [4,5]. Fidelity of transcription is a multistep process controlled at the nucleotide addition cycle and slow misincorporation allows exchange by the correct base in case of multisubunit RNA polymerases (RNAPs). The incorrect bases are removed with factors that stimulate 3′ RNA cleavage activity such as Gre factors in bacterial enzymes and TFIIS in human RNAPII. Thus, the multisubunit RNAP achieves fidelity through substrate selection and proofreading. Restructuring of the trigger loop in RNAPII has been shown to be essential for efficient catalysis of the phosphodiester bond which occurs solely in the presence of complementary nucleotide triphosphate [6,7].

In addition to the nucleus, the mitochondria and plastids also possess their own genomes and transcription machinery. Single-subunit RNAPs are involved in transcription of small genomes in mitochondria, plastids, and phages. Mitochondria are involved in the ATP production for the cell, the by-products of which are the reactive oxygen species (ROS) such as hydrogen peroxide, superoxide, and singlet oxygen. ROS can damage the nucleic acids and their precursor ribonucleotides (NTPs) such as GTP and ATP resulting in the formation of 8-oxo-GTP and 2-hydroxy-ATP, respectively. 8-Oxo-GTP, the product of guanosine oxidation, is known to accumulate in the mitochondrial DNA under pathological conditions and during aging [8,9]. 8-Oxo-guanine also gets incorporated into

RNA leading to transcriptional and translational errors [10,11]. Although there have been studies regarding the incorporation of 8-oxo-guanine and 2-hydroxy-adenine into RNA by the multisubunit RNAP from *E. coli* and human [12], there is no such study on the single-subunit RNAPs.

The transcriptional mutagenesis can also be induced when oxidatively damaged DNA templates are bypassed by RNAPs. *In vitro* studies have shown that the RNAP can efficiently bypass the nonbulky lesions, with base misinsertion leading to transcriptional mutagenesis [13,14]. However, the RNAPs also get permanently stalled when they encounter bulky lesions in DNA [15].

The mitochondrial transcription in *Arabidopsis thaliana* is mediated by two nuclear-encoded single-subunit (~100 kDa) RNAPs − RpoTm and RpoTmp [16]. While RpoTmp transcribes a subset of mitochondrial genes that are not defined by a common promoter sequence, RpoTm is the primary RNAP in the mitochondria and is essential for plant development. RpoTm is 976 amino acid (110 kDa)−containing enzyme which is required for the transcription of most of the mitochondrial genes including those that are involved in the oxidative phosphorylation for ATP generation. Its deletion is lethal to the plant [17,18]. There is no report on the transcriptional fidelity and efficiency of incorporation of correct and incorrect bases by any of the plant RNAPs.

In the present study, we have carried out a comprehensive characterization of the nucleotide selectivity of the mitochondrial RNAP of *Arabidopsis thaliana* − RpoTm by examining its transcriptional fidelity. In addition, we probe the propensity of RpoTm to misincorporate unmodified as well as oxidized nucleotides into RNA and for translesion bypass on oxidatively damaged DNA template. Our study reveals that fidelity of RpoTm is akin to the other single-subunit RNAPs and is higher than that of multisubunit RNAP of *Escherichia coli*. In addition, RpoTm has lower efficiency for addition of oxidatively damaged ribonucleotides into RNA as opposed to normal bases. The rates of addition of oxidatively damaged ribonucleotides into RNA are comparable to the mismatch frequency. Homology modeling allowed identification of residues which when mutated compromise the transcription efficiency of the enzyme.

Results

Purified RpoTm extends RNA in the primer extension assay in the presence of Mg^2

The *Arabidopsis thaliana* single-subunit mitochondrial RNAP RpoTm without the mitochondrial targeting peptide was overexpressed in *E. coli* as a fusion protein with N-terminus His tag. Site-specific cleavage by the PreScission Protease was carried out to remove the tag. We developed promoter-free *in vitro* transcription assay using a synthetic DNA:RNA hybrid for analysis of the kinetics of incorporation of nucleotides by RpoTm. The scaffold consists of a 38-nucleotide-long template DNA annealed to an eight-nucleotide-long 5′ 6-FAM−labeled RNA and a 38-nucleotide-long nontemplate strand forming a 9bp melted region (transcription bubble). The DNA:RNA hybrid in Fig. 1a contains thymine as the +1 template base (ES8T). It was observed that, in the presence of NTP mix and increasing concentrations of RpoTm, the RNA gets extended in a template-dependent fashion (Fig. 1b, lane 2, 3, and 4). Based on sequence alignment with T7 RNAP, D909 and D677 were identified as the two conserved catalytic residues. The residues corresponding to D909 and D677 in T7 RNAP form coordination bonds with the two Mg^{2+} ions in the crystal structure [19]. In RpoTm, the substitution of D909 to alanine (D909A) fails to extend RNA, confirming that the catalytic activity observed is specific to RpoTm (Fig. 1b lane 5, 6, and 7). This also rules out that the RNA extension activity might be due to contaminating nucleic acid polymerase.

Full-length protein was unstable and prone to aggregation. Sequence alignment of RpoTm with the extensively studied T7 RNAP shows that plant protein is longer by 57 amino acids at the N-terminus. Secondary structure prediction server PSIPRED [20] predicts that this region is disordered in RpoTm. A smaller construct of RpoTm (58−976 amino acids − 101 kDa- ΔRpoTm) was thus designed by sequence alignment with T7 RNAP (Fig. S1a). ΔRpoTm was purified using the same protocol as the full-length protein. Compared with the full-length protein, the shorter construct was more soluble and less prone to aggregation, resulting in five-fold more protein as compared with the full-length RpoTm (Fig. S1b). N- and C-terminus truncations have been known to stabilize proteins [21]. The *in vitro* transcription assay with the ΔRpoTm shows activity comparable with the full-length construct (Fig. 1c). Hence, all further experiments were performed with the truncated construct.

To test if the transcription activity was metal dependent, the assay was performed in the presence and absence of Mg^{2+} ions. No extension was observed in the absence of Mg^{2+} ions demonstrating that the activity of RpoTm is metal ion−dependent, analogous to T7 RNAP (Fig. 1d). We next measured the equilibrium dissociation constant (K_d) and off-rate (k_{off}) of ΔRpoTm for the ES8T nucleic acid scaffold using fluorescence anisotropy experiments. To determine the affinity (K_d), 5 nM of the scaffold (ES8T) was titrated against increasing concentration of the enzyme (Fig. 1e). The K_d was

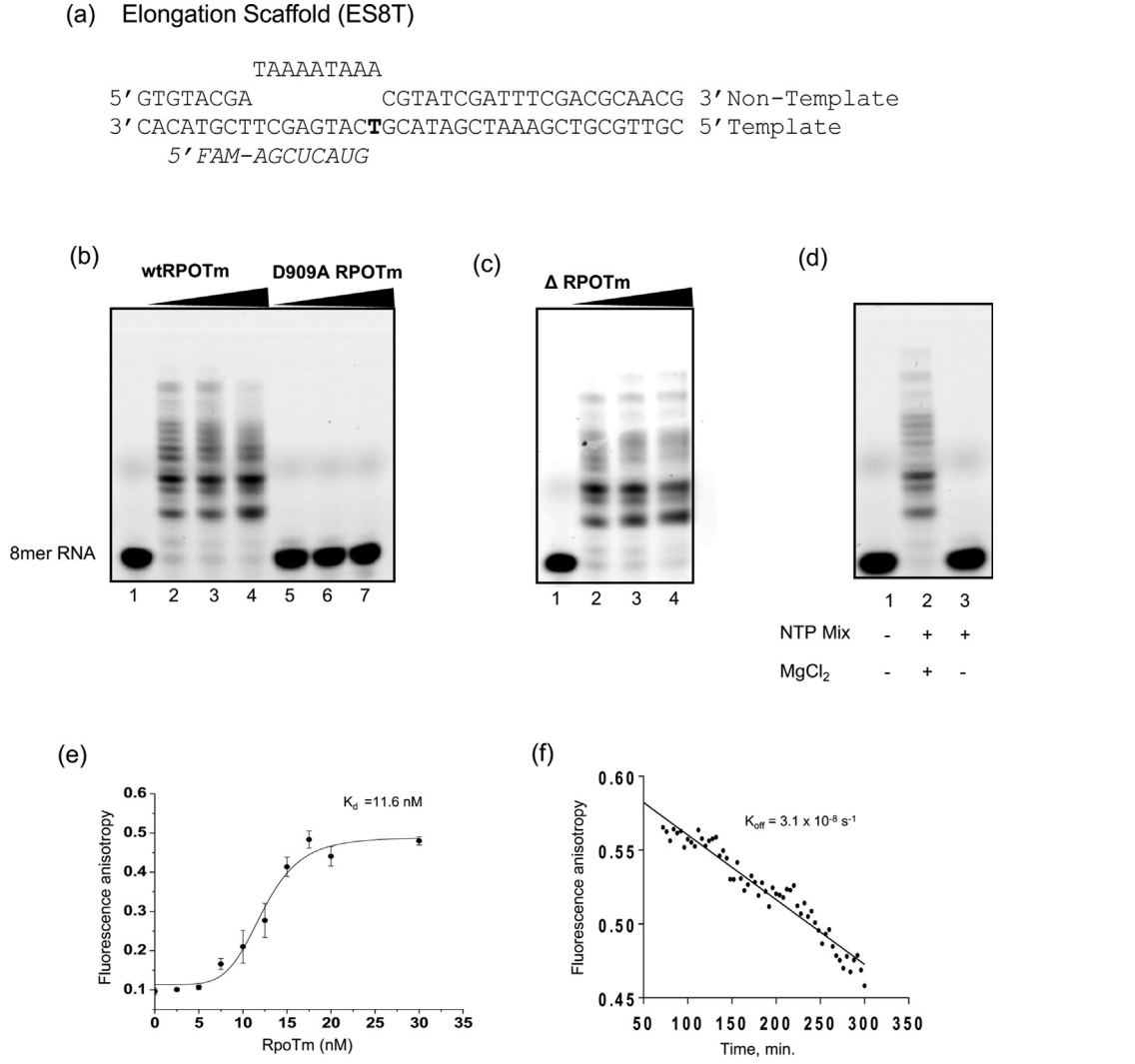

Fig. 1. Activity of RpoTm (a) The DNA:RNA scaffold used in the assay is shown. The eight base RNA is 5′ 6-FAM labeled and is shown in italics. The dsDNA is 38 nucleotides long with 9bp melted region. The base in bold in DNA is the templating base. (b) The gel image showing the elongation of 8-mer RNA using ES8T (300 nM) and 10 μM NTP in a reaction containing either 0.25 μM (lane 2) 0.5 μM (lane 3), 1 μM (lane 4) of full-length wtRpoTm, or 0.25 μM (lane 5), 0.5 μM (lane 6), and 1 μM (lane 7) of mutant RpoTm (D909A). Lane 1 shows no enzyme control (c) The gel image showing products of the reaction containing ES8T (300 nM) in the presence of 0.25 μM (lane 2), 0.5 μM (lane 3), and 1 μM (lane 4) of ΔRpoTm. Lane 1 is no enzyme control (d) The gel shows the effect of metal ions on the activity of ΔRpoTm. Reaction products in the presence of ES8T (300 nM) and 0.5 μM of ΔRpoTm in the presence (lane 2) and absence (lane 3) of 15 mM $MgCl_2$ are shown. No enzyme control is in lane 1. (e) The plot showing fluorescence anisotropy of 5 nM FAM-labeled ES8T complex in the presence of increasing concentration of the enzyme. (f) The plot depicting fluorescence anisotropy as a function of time when a complex of 6-FAM−labeled ES8T (5 nM) and ΔRpoTm (60 nM) is chased with unlabeled ES8T (500 nM).

calculated to be 11.6 nM, confirming a high-affinity complex. The off-rate of the complex was calculated by adding excess of unlabeled scaffold to a preformed complex of ΔRpoTm with the labeled scaffold (Fig. 1f). Time-dependent decrease in anisotropy was recorded and a dissociation rate of $3.1 \times 10^{-8}\ s^{-1}$ was observed as would be expected for a high-affinity complex.

Fidelity and mismatch frequency of RpoTm

The study on the fidelity of the other single-subunit polymerases (T7, POLRMT, and Rpo41) shows that the transcriptional accuracy is comparable with that of the fidelity of DNA polymerases in the absence of DNA mismatch repair [22,23]. However, this analysis has not been carried out for any of the plant

mitochondrial polymerases. To ascertain the stringency of the substrate specificity of RpoTm, assays were performed with four different promoter-free DNA:RNA scaffolds, where one of the four bases was present at the template position (ES8A, ES8T, ES8G, and ES8C) and in the presence of only one NTP at a time (Fig. 2a). ΔRpoTm incorporated the correct nucleotide opposite to template base for all ES8 complexes (Fig. 2b). Steady-state kinetics was performed and kinetic parameters (K_m, V_{max}, K_{cat}) were determined for all cognate (Watson-Crick) and noncognate base pairs formed (a representative Michaelis-Menten and Lineweaver-Burk plots are shown in Fig. S2). For all incoming Watson-Crick base pairings, the K_m values were found to be in the range of 30−90 nM (Table 1). The catalytic efficiency for correct nucleotide incorporation was found to be in the range of about 1240.7−4957.8 $min^{-1}mM^{-1}$.

Noncognate insertions into the RNA were also observed. Compared with all other bases, cytosine in the template position shows the lowest fidelity, with ATP, UTP, and CTP misincorporations (Fig. 2a: lane 21, 22, and 24). However, the kinetics reveals that the catalytic efficiency of the miscoding was low with the mismatch efficiency of dC:ATP and dC:UTP being 63-fold and 328-fold lower, respectively, than that of cognate pairing (Table 2). The ratio of the insertion efficiency of the incorrect and correct base pair indicates the misinsertion frequency (f) or the error rate of the polymerase. The mismatch frequency for dC:ATP and dC:UTP was calculated to be 15×10^{-3} and 3×10^{-3}, respectively.

Similarly, for dT as the template, UTP, GTP, and CTP were misincorporated (lane 10, 11, and 12) (Fig. 2a). Amongs these, the efficiency of dT:GTP misincorporation was calculated to be 23.2 $min^{-1}mM^{-1}$, about 135-fold lower than that of cognate (dT: ATP) pairing with the error rate of 7×10^{-3}. For dA templating base ATP, GTP, and CTP (Fig. 2a: lane 3, 5, and 6) and for dG template low amounts of

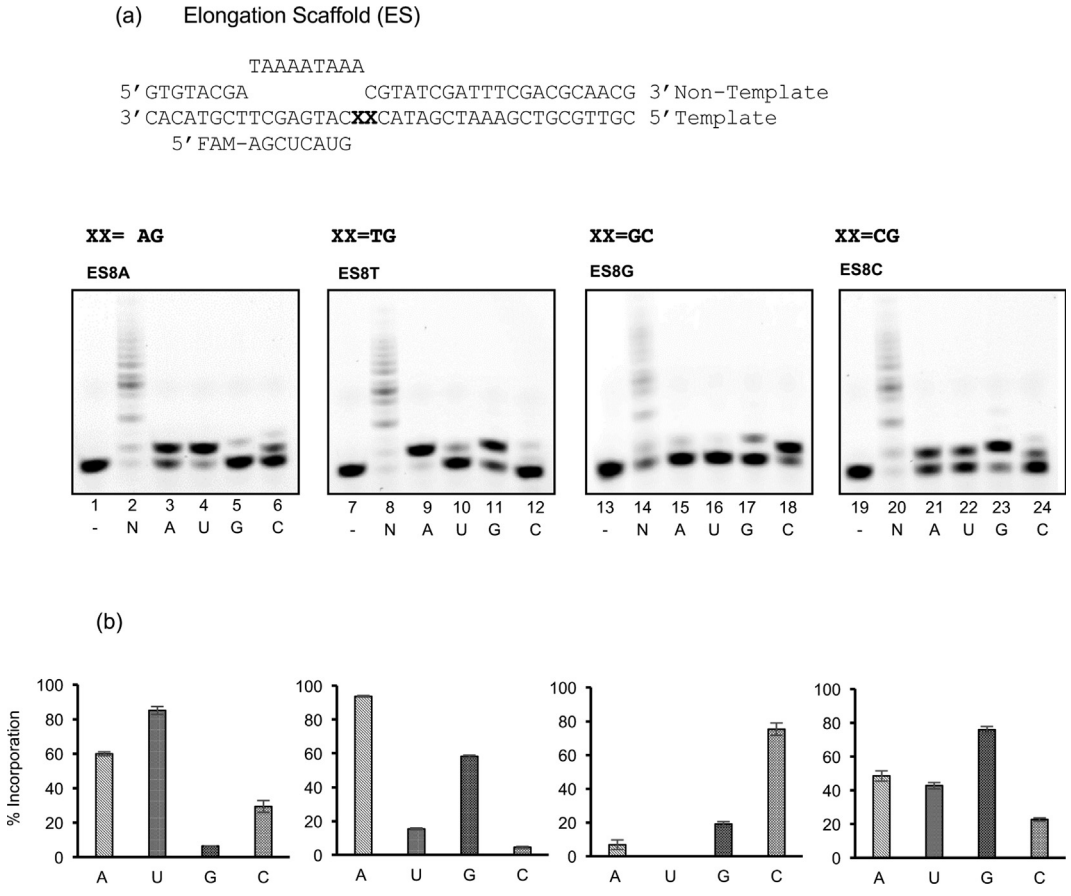

Fig. 2. The fidelity profile of ΔRpoTm toward NTPs (a) The DNA:RNA hybrid used in the assay is shown. The template base and the adjacent base (in bold) on DNA is depicted for each gel. The gel image showing the products of single nucleotide addition by ΔRpoTm in the presence of different DNA:RNA hybrids at 150 nM incubated with either no NTP (lane 1, 7, 13, and 19) or 2 μM of NTP (lane 2, 8, 14, and 20) or ATP (2 μM) (lane 3, 9, 15, and 21) or UTP (2 μM) (lane 4, 10, 16, and 22) or GTP (2 μM) (lane 5, 11, 17, and 23) or CTP (2 μM) (lane 6, 12, 18, and 24), respectively. (b) The bar diagram showing the percentage incorporation of each of the four nucleotides against the four template bases by ΔRpoTm.

Table 1. Table showing K_m, K_{cat}, and catalytic efficiency of ΔRpoTm for insertion of cognate nucleotides.

Base pair	K_m (μM)	K_{cat} (min^{-1})	K_{cat}/K_m ($min^{-1}mM^{-1}$)
dT: ATP	0.08 ± 0.005	0.24 ± 0.005	3133.8
dA: UTP	0.09 ± 0.011	0.12 ± 0.011	1240.7
dC: GTP	0.03 ± 0.002	0.17 ± 0.002	4957.8
dG: CTP	0.08 ± 0.005	0.16 ± 0.013	2034.7

ATP and GTP (Fig. 2a lane 15 and 17) were misincorporated. The efficiencies of RpoTm for dA:ATP and dG:GTP mismatches were 459-and 56-fold lower than that of cognate base pair, respectively. The error rates for these were calculated to be 2×10^{-3} and 18×10^{-3}, respectively. The kinetic measurements could not be performed for other mismatches because product at lower enzyme concentrations could not be quantified and multiple bands were observed on the gel at higher enzyme concentrations, showing RNA extension beyond misincorporation.

Complete data on fidelity by RpoTm indicate that the catalytic efficiency of misincorporations by RpoTm is about 10^3-fold lower than that of correct pairing. In addition, the K_m values of incorrect pairings were about 100-fold higher than that of correct pairing. Overall, the U to A and G to U errors are more frequent for RpoTm.

Incorporation of oxidized nucleotides into RNA by RpoTm

Incorporation and extension beyond oxidized nucleotides of RNA by any single-subunit RNAPs have not been documented thus far. The ability of RpoTm to incorporate 8-oxo-GTP into RNA opposite different templating nucleotides (ES8A, ES8T, ES8G, and ES8C) was investigated. It was observed that the ΔRpoTm was able to insert 8-oxo-GTP opposite to dA, dC, and dT (Fig. 3a, lane 3, 4, and 6). While 8-oxo-GTP can base pair with C through Watson-Crick pairing, it can base pair efficiently with A through Hoogsteen base pairing by adopting a *syn* conformation, triggered by steric repulsion between the 8-oxo group and the O4′ oxygen atom [24]. However, the K_m of ΔRpoTm for 8-oxo-GTP is 154- and 88-fold higher against dC and dA, respectively, as compared with unmodified nucleotides (Table 3). Similarly, the catalytic efficiency of the enzyme is 117- and 50-fold less than that of the incorporation of unmodified nucleotides (Fig. 3b and Table 3). The error rate for the incorporation of 8-oxo-GTP against dC, dA, and dT was calculated to be 8.5×10^{-3}, 20×10^{-3}, and 1.5×10^{-3}, respectively. These error rates are similar to the mismatch frequency calculated above.

We tested the ability of ΔRpoTm to incorporate another commonly occurring oxidatively damaged nucleotide 2-hydroxy-ATP opposite to different templating nucleotides (ES8A, ES8T, ES8G, and ES8C). It was observed that RpoTm incorporated 2-hydroxy-ATP correctly opposite to dT (Fig. 3c, lane 4). Incorporations against dA and dC were also observed (lane 3 and 6). Subsequently, the kinetic analysis reveals that the apparent affinity (K_m) of ΔRpoTm for 2-hydroxy-ATP was approximately 21-fold less than that of ATP and catalytic efficiency for the incorporation of oxidized ATP against dT is about 31-fold less than that of unmodified NTP (Fig. 3d and Table 4). The error rate of 2-hydroxy-ATP insertion into RNA is 3×10^{-2}, highest for any noncognate incorporation tested. Oxidized ATP was also seen to be incorporated against dC and dA with very low efficiency.

Thus, data on insertion of oxidized nucleotides into RNA by RpoTm show that the polymerase has a similar propensity of insertion of oxidized bases into RNA as compared with noncognate bases with higherpropensity for insertion of 2-hydroxy-ATP.

Incorporation of oxidized nucleotides into RNA by T7 RNAP

Multisubunit RNAP from *E. coli* has lower K_m in nucleotidyl transfer reaction for 8-oxo-GTP incorporation opposite to template dA and dC than that of normal NTP [12], which is contrary to what was observed for RpoTm. To generalize if it is the case with other single-subunit RNAPs, we investigated the ability of T7 RNAP to incorporate oxidized nucleotides into RNA. We procured T7 RNAP from New England Biolabs (catalog number M0251S) and

Table 2. Table showing K_m, K_{cat}, catalytic efficiency, and error frequency of ΔRpoTm for insertion of noncognate nucleotides.

Base pair	K_m (μM)	K_{cat} (min^{-1})	K_{cat}/K_m ($min^{-1}mM^{-1}$)	Transcriptional error rates (K_{cat}/K_m) incorrect/(K_{cat}/K_m) correct)
dA: ATP	8.0 ± 0.4	0.02 ± 0.002	2.7	2×10^{-3}
dT: GTP	8.3 ± 1.4	0.19 ± 0.02	23.2	7×10^{-3}
dG:GTP	0.5 ± 0.05	0.02 ± 0.001	36.5	18×10^{-3}
dC: ATP	1.9 ± 0.02	0.15 ± 0.002	78.6	15×10^{-3}
dC: UTP	15.9 ± 3.8	0.23 ± 0.024	15.1	3×10^{-3}

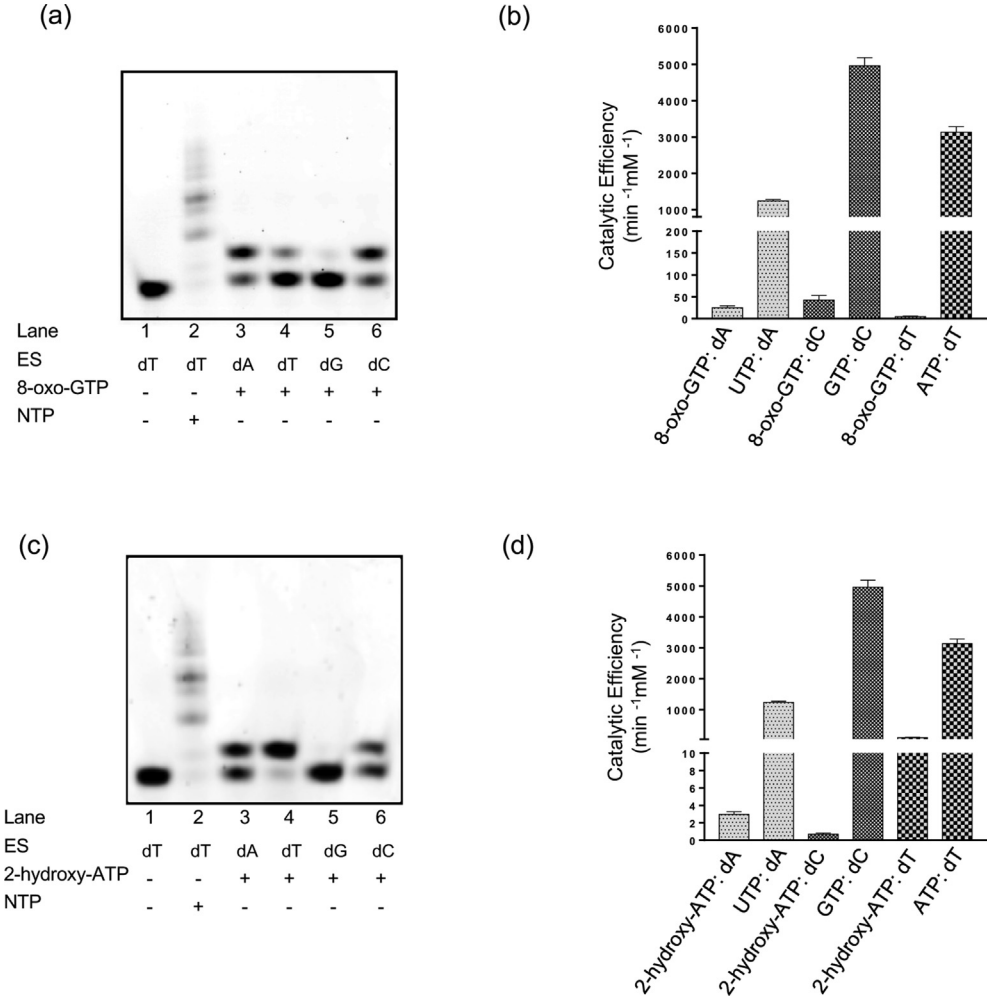

Fig. 3. Incorporation of 8-oxo-GTP and 2-hydroxy-ATP by ΔRpoTm: The gel image showing the addition of (a) 8-oxo-GTP and (c) 2-hydroxy-ATP against each of the four template nucleotide by 150 nM of ΔRpoTm.150 nM of scaffold was incubated with no NTP (lane 1), all NTP (2 μM) (lane 2), and oxidized nucleotides (2 μM) (lane 3, 4, 5, and 6). (b) The bar diagram showing the comparison of catalytic efficiency of ΔRpoTm for incorporating 8-oxo-GTP and correct NTPs (d) The bar diagram showing the comparison of catalytic efficiency of ΔRpoTm for incorporating 2-hydoxy-ATP and correct NTPs.

Table 3. Table showing K_m, K_{cat}, catalytic efficiency, and error frequency of ΔRpoTm for insertion of 8-oxo-GTP.

Base pair	K_m (μM)	K_{cat} (min^{-1})	K_{cat}/K_m ($min^{-1}mM^{-1}$)	Transcriptional error rates ((K_{cat}/K_m) incorrect/(K_{cat}/K_m) correct)
dA: 8-oxo-GTP	7.9 ± 1.15	0.19 ± 0.007	24.9	20×10^{-3}
dC: 8-oxo-GTP	4.63 ± 0.84	0.19 ± 0.024	42.3	8.5×10^{-3}
dT: 8-oxo-GTP	4.48 ± 0.22	0.02 ± 0.004	4.9	1.5×10^{-3}

Table 4. Table showing K_m, K_{cat}, catalytic efficiency, and error frequency of ΔRpoTm for insertion of 2-hydroxy-ATP.

Base pair	K_m (μM)	K_{cat} (min^{-1})	K_{cat}/K_m ($min^{-1}mM^{-1}$)	Transcriptional error rates ((K_{cat}/K_m) incorrect/(K_{cat}/K_m) correct)
dT: 2-hydroxy-ATP	1.7 ± 0.07	0.17 ± 0.021	102	3×10^{-2}
dC:2-hydroxy-ATP	87.7 ± 24.2	0.06 ± 0.005	0.7	2×10^{-4}
dA: 2-hydroxy-ATP	13.8 ± 4.9	0.04 ± 0.01	3	9×10^{-4}

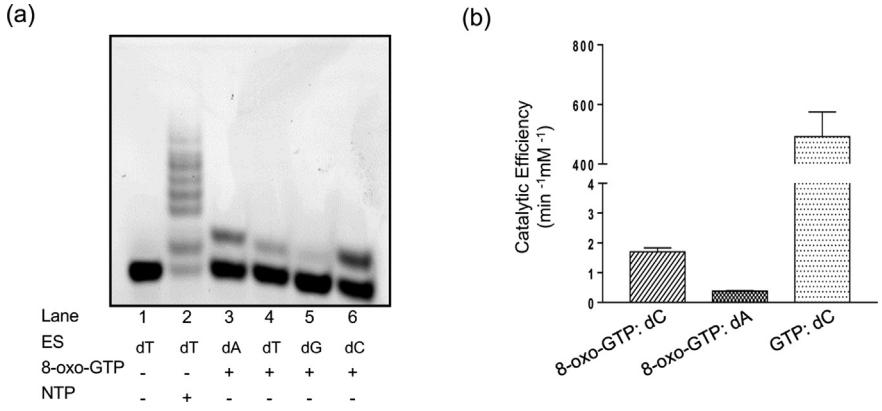

Fig. 4. Incorporation of 8-oxo-GTP by T7 RNAP: (a) The gel image showing the addition of 8-oxo-GTP against each of the four template nucleotide by 300 nM of T7 RNAP. 150 nM of scaffold was incubated with no NTP (lane 1), all NTP (50 μM) (lane 2) and oxidized nucleotide (50 μM) (lane 3, 4, 5, and 6). (b) The bar diagram showing the comparison of catalytic efficiency of T7 RNAP for incorporating 8-oxo-GTP against dA and dC and cognate base pair.

generated the fidelity profile for the incorporation of 8-oxo-GTP. As observed in the case of RpoTm, T7 RNAP predominantly incorporated 8-oxo-GTP opposite to dA and dC (Fig. 4a). The efficiency of incorporation of 8-oxo-GTP against dA and dC was 1294- and 289-fold lower than that of GTP against dC (Fig. 4b and Table 5). Thus, the T7 RNAP is more stringent for 8-oxo-GTP insertion compared with RpoTm. This also implies that the lower rate of incorporation of oxidized bases into RNA may be a general feature of single-subunit RNAPs.

Unlike multisubunit RNAPs and replicative DNA polymerase, proofreading activity has not been reported for single-subunit RNAPs [25]. To determine if the polymerase stalls or bypasses the oxidized nucleotides in RNA, we assayed for RNA elongation after 8-oxo-GTP incorporation by RpoTm using ES8C (Fig. 5a). When NTP mix or the ribonucleotide complementary to the +2 position was added 5 min after the 8-oxo-GTP was incubated with the enzyme, further extension of RNA beyond the incorporation of the oxidized nucleotide was observed (Fig. 5a, lane 6 and 7). Addition of NTP 5 min after preincubation with GTP (+1 nucleotide) shows extension similar to where only NTPs have been added (Fig. 5a, lane 3 and 4). Thus, the enzyme was able to bypass the misincorporated 8-oxo-GTP. Similar results were obtained with 2-hydroxy-ATP where RpoTm extended the RNA beyond addition of 2-hydroxy-adenine (Fig. 5b, lane 6 and 7). This indicates that these insertions are expected to lead to mutations in the RNA. In contrast, the multisubunit RNAPs and DNA polymerases are known to slow down, and their proofreading activity is stimulated in the presence of mismatches [26].

8-oxo-guanine bypass by RpoTm is associated with transcriptional mutagenesis

Apart from the oxidation of endogenous NTP pool, the mitochondrial DNA is also under the attack from the oxidative environment. Most abundant DNA lesions in oxidative environments are 8-oxo-guanine, 8-oxo-adenine, and apurinic/apyrimidinic (AP) base. The ability of RpoTm to bypass these lesions was assessed using a minimal scaffold. The DNA template containing three different DNA lesions at the 9th position of template DNA were hybridized to a 6-FAM–labeled 8-mer RNA and standing start reactions were performed. Addition of few bases was observed for DNA template containing AP site and 8-oxo-adenine in the presence of NTPs (Fig. 6a and b, lane 2). Only a few bases were added after the DNA lesion followed by either stalling or termination of the reaction (Fig. 6a and b). When single NTP was used opposite to the AP DNA lesion, only ATP was seen to get incorporated. Interestingly, a majority of the replicative and repair DNA polymerases stall at the abasic site followed by predominantly inserting adenine opposite to it. This strong preference for adenine as also observed in RpoTm is referred to as the A-rule [27].

Table 5. Table showing K_m, K_{cat}, catalytic efficiency, and error frequency of T7 RNAP for insertion of 8-oxo-GTP.

Base pair	K_m (μM)	K_{cat} (min^{-1})	K_{cat}/K_m ($min^{-1}mM^{-1}$)	Transcriptional error rates ((K_{cat}/K_m) incorrect/(K_{cat}/K_m) correct)>
dC: 8-oxo-GTP	34.7 ± 2.0	0.06 ± 0.001	1.7	3.4×10^{-3}
dA: 8-oxo-GTP	79.6 ± 1.9	0.03 ± 0.002	0.38	7.7×10^{-4}
dC: GTP	0.09 ± 0.002	0.04 ± 0.002	492	

(a) Elongation Scaffold (ES8C)

```
          TAAAATAAA
5′GTGTACGA         CGTATCGATTTCGACGCAACG 3′Non-Template
3′CACATGCTTCGAGTACCGCATAGCTAAAGCTGCGTTGC 5′Template
    5′FAM–AGCUCAUG
```

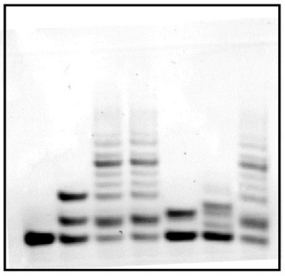

Lane	1	2	3	4	5	6	7
8-oxo-GTP	-	-	-	-	+	+	+
GTP	-	+	-	+	-	-	-
CTP after 5min	-	+	-	-	-	+	-
NTP	-	-	+	-	-	-	-
NTP after 5min	-	-	-	+	-	-	+

(b) Elongation Substrate (ES8T)

```
          TAAAATAAT
5′GTGTACGA         CGTATCGATTTCGACGCAACG 3′Non-Template
3′CACATGCTTCGAGTACTGCATAGCTAAAGCTGCGTTGC 5′Template
    5′FAM–AGCUCAUG
```

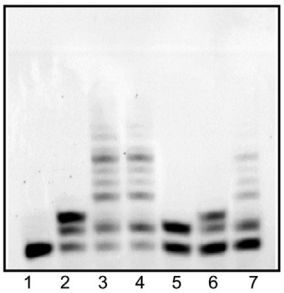

Lane	1	2	3	4	5	6	7
2 Hydroxy-ATP	-	-	-	-	+	+	+
ATP	-	+	-	+	-	-	-
CTP after 5min	-	+	-	-	-	+	-
NTP	-	-	+	-	-	-	-
NTP after 5min	-	-	-	+	-	-	+

Fig. 5. E**xtension beyond inserting of 8-oxo-GTP and 2-hydroxy-ATP by ΔRpoTm:** (a) The DNA:RNA scaffold used in the experiment is depicted at the top. The 5′-FAM–labeled RNA is in italics, the template base is in bold. The gel showing the extension of ES8C (150 nM) in the presence of 150 nM ΔRpoTm where no NTP (lane 1), 5 μM GTP (lane 2, 4), 5 μM NTP (lane 3), and 5 μM 8-oxo-GTP (lane 5, 6, and 7) was used. Lane 2 and 4 were preincubated with GTP (5 μM) for 5 min followed by the addition of CTP (5 μM) and NTP (5 μM), respectively. Lane 6 and 7 were preincubated with 8-oxo-GTP (5 μM) for 5 min followed by addition of CTP (5 μM) and NTP (5 μM), respectively. (b) The DNA:RNA scaffold used in the experiment is depicted at the top. The 5′-FAM–labeled RNA is in italics, the template base is in bold. The gel showing extension of ES8T (150 nM) in the presence of 150 nM ΔRpoTm where no NTP (lane 1), 5 μM ATP (lane 2, 4), 5 μM NTP (lane 3), and 5 μM 2-hydroxy-ATP (lane 5, 6, and 7) was used. Lane 2 and 4 were preincubated with ATP (5 μM) for 5 min followed by the addition of CTP (5 μM) and NTP (5 μM), respectively. Lane 6 and 7 were preincubated with 2-hydroxy-ATP (5 μM) for 5 min followed by the addition of CTP (5 μM) and NTP (5 μM), respectively.

(a)
5′ FAM-AGCUCAUG
3′ TCGAGTAC**[AP]**CATAGCTAAAGCTGCGTTGC5′

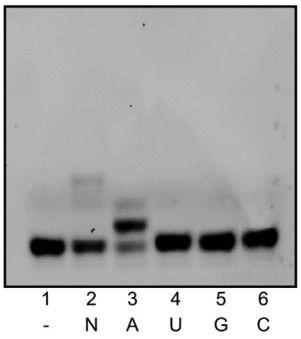

(b)
5′FAM-AGCUCAUG
3′ TCGAGTAC**[8-oxo-dA]**CATAGCTAAAGCTGCGTTGC5′

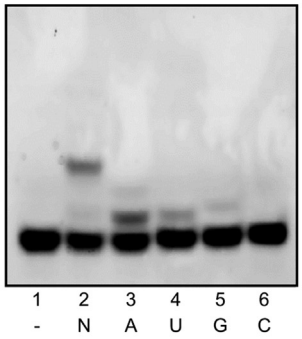

(c)
5′FAM- AGCUCAUG
3′ TCGAGTAC**[8-oxo-dG]**CATAGCTAAAGCTGCGTTGC5′

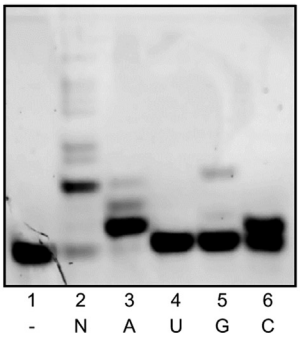

Fig. 6. DNA lesion bypass by ΔRpoTm: The gel pictures showing extension using DNA:RNA scaffolds with (a) abasic lesion, (b) 8-oxo-adenine lesion, and (c) 8-oxo-guanine lesion. The scaffolds were incubated with 50 μM of no NTP (lane 1), NTP (lane 2), ATP (lane 3), UTP (lane 4), GTP (lane 5), and CTP (lane 6). Reactions were initiated by adding 300 nM of ΔRpoTm and incubating for 30 min at 27 °C.

T7 RNAP, *E. coli* RNAP, and mammalian and yeast RNAPII are all known to bypass 8-oxo-guanine in DNA [28–31]. T7 RNAP also prefers to add adenine opposite to 8-oxo-guanine. *E. coli* and yeast RNAP II incorporate both adenine and cytosine with similar efficiencies. In case of RpoTm, ATP and CTP were seen to be efficiently incorporated opposite to 8-oxo-guanine lesion in the DNA strand (Fig. 6c, lane

3, 6). This behavior is also similar to the human mitochondrial RNAP (POLRMT) that incorporates ATP and CTP opposite to 8-oxo-guanine DNA lesion as seen in pre−steady-state kinetics [23]. This indicates that possibly the template base is present in *syn* conformation for the formation of the stable Hoogsteen base pair with the incoming adenine, leading to misincorporations. Incubation of enzyme-scaffold complex with NTP led to RNA extension (Fig. 6c, lane 2) demonstrating that the lesion does not block RpoTm during elongation. Thus, it can be concluded that the transcriptional bypass of 8-oxo-gaunine by RpoTm will be associated with C to A mutagenesis in RNA.

Modeling of RpoTm aids in the identification of the residues that stabilize the incoming and template nucleotide

Crystal structure of single-subunit mitochondrial RNAP from *Arabidopsis thaliana* is not available. To delineate the residues that stabilize the incoming and the template nucleotide, a homology-based model of elongation complex was constructed. The protein sequence of RpoTm was obtained from the National Center for Biotechnology Information database. The full-length RpoTm shares 35% and 29% identity with POLRMT and T7 RNAP, respectively. Sequence alignment with T7 and POLRMT shows that RpoTm is a two-domain protein the N-terminus domain (NTD) and a C-terminus domain (CTD) (Fig. S3). RpoTm has an extension at the amino terminus (residues 1−57) that is absent in T7 RNAP. This region does not show any significant homology with the N-terminus region of hPOLRMT and hence could not be modeled in RpoTm. The NTD, which has been shown to be vital for promoter recognition for T7 RNAP and POLRMT [32,33], differs considerably in length and sequence between the three proteins particularly, the two functional loops, the recognition region and the intercalating hairpin which are essential for promoter binding and promoter melting, respectively, in T7 RNAP [19,34]. The recognition loop is longer in RpoTm compared with the other two polymerases. The CTD, which shares high sequence homology with T7 and hPOLRMT, adopts a "right-handed topology" with the three major domains − fingers (693−845), palm (407−462, 546−692, 867−976), and the thumb (463−545). The palm domain accommodates the catalytic centre of the enzyme with the two conserved catalytic residues (D909 and D677) which coordinate the metal ion and come close to the 3′ end of the RNA.

We modeled RpoTm using the elongation complex crystal structure of T7 RNAP (PDB: 1S76) which includes the NTP substrate and metal ion (Fig. 7a). The metal ion and the incoming substrate are absent in the elongation complex of human mitochondrial RNAP structure which is in the pretranslocation state where the 3′ terminal RNA nucleotide occupies the site for the incoming nucleotide. We built separate models where the incoming nucleotide was replaced with either the 8-oxo-GTP or 2-hydroxy-ATP. Mg^{2+} ions were included in the models. The models show that the incoming 8-oxo-GTP will form the Hoogsteen base pairing with the template base dA. The 2-hydroxy-ATP, on the other hand, forms Watson-Crick base pairing with the template thymine.

Alanine substitutions of the residues that stabilize the template or the incoming nucleotide are defective in transcription

Based on the homology model (Fig. 7a), the residues that contact the incoming as well as the template nucleotides, were identified and substituted

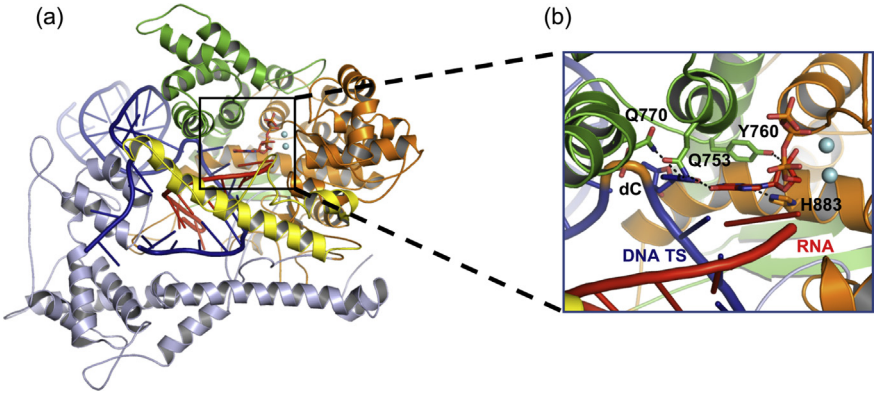

Fig. 7. Homology Model of ΔRpoTm: (a) The model of ΔRpoTm is shown in ribbon representation. The NTD (gray), finger (green), palm (orange), and thumb (yellow) domains are colored. The DNA is shown as blue sticks and RNA is in red. (b) Zoomed in view of the active site is depicted. The Mg^{2+} ions are seen as cyan spheres. The incoming nucleotide is shown in stick representation. The side chains of the residues interacting with the incoming and template nucleotides are shown.

with alanine to evaluate their effect on the overall transcriptional activity as well as fidelity toward incorporation of oxidized ribonucleotides. Fig. 7b shows the active site of the RpoTm in the model. Based on the model, a total of five mutants were prepared (numbers in parenthesis are for corresponding residues in T7 RNAP and POLRMT, respectively) – Q770A (Q649, Q1009), Q753A (R632, Q992), Q753R (R632, Q992), H883A (H784, H1125), and Y760A (Y639, Y999). Based on the sequence alignment with T7 RNAP and POLRMT, the residues Q770, Q753, and Y760 of RpoTm are present in the finger subdomain whereas H883 is located in the palm subdomain. Transcription assay was carried out with the mutant enzymes. All the mutants were impaired for their transcription ability in the presence of all NTPs (Fig. 8, lane 2). The mutants were also assessed for their ability to incorporate 8-oxo-GTP and 2-hydroxy-ATP into RNA. Incorporation was tested against all the four templating bases (dA, dT, dG, and dC). The results revealed that all the mutants incorporated 8-oxo-GTP opposite to dA and dC (Fig. 8a, lane 3 and 6) although with severely compromised efficiency compared with the wild-type enzyme, indicating that the identified amino acid residues are essential for stabilization of the oxidized NTP substrate. Significant 2-hydroxy-ATP was seen to be incorporated opposite to dT as seen for the wild-type RpoTm (Fig. 8b, lane 4). A plot showing percentage insertion of 2-hydroxy-ATP by wtΔRpoTm and the mutants shows that substitution of Q753A has mild effect on insertion of 2-hydroxy-ATP compared with wtRpoTm and Q770A substitution is impaired for incorporation of oxidized nucleotide opposite to dT (Fig. 8c).

Similar residues in T7 RNAP have been implicated in transcriptional fidelity. Residue Y639 has been determined to be critical for differentiating between the ribonucleotide and deoxyribonucleotide. Substitution of Y639F in T7 RNAP reduces the ability of the RNAP to discriminate between the rNTPs and dNTPs while substitution of Y639A causes loss of activity [35]. Similarly, substitution of H784 with alanine in T7 RNAP is associated with a slower rate of misincorporation but increased mismatch extension [36]. The Q649S substitution in T7 causes modest reduction in K_m for various NTPs [37,38]. The R632G mutation in T7 RNAP is known to reduce the overall activity of the enzyme [39].

Discussion

The fidelity of an RNAP is primarily determined at the selection step of the correct nucleotide over the incorrect nucleotide. The RNAP forms the complex with DNA and this is followed by magnesium-mediated incorporation of the incoming nucleotide on to the 3′ prime end of RNA thereby increasing the length of growing RNA chain by one nucleotide and release of PPi [33]. Multisubunit RNAPs possess RNA proofreading activity among them is the intrinsic RNA cleavage activity where, in the event of misincorporation, the polymerase backtracks and a 3′ terminal transcript segment containing noncognate nucleotide residue is cleaved [40]. In yeast, the transcription elongation factor S-II interacts with stalled RNAPII after misincorporations in the nascent mRNA. S-II relieves the arrest by stimulating the cleavage of the incorrect base [41].

A detailed mechanism of how the cells handle oxidatively damaged RNA under normal physiological conditions remains largely unexplored, although enzymes such as polynucleotide phosphorylase in *E. coli* and YB1 in human are known to scavenge oxidatively damaged RNA [42]. On the other hand, oxidized bases in the DNA are repaired in bacterial and mammalian cells by enzymes that are involved in the base excision repair (BER) pathway which can excise 8-oxo-guanine from DNA [43]. These enzymes are localized in both the nucleus and mitochondria and include adenine DNA glycosylase (homolog of MutY) and 8-oxo-guanine DNA glycosylase/lyase (OGG). These enzymes function together to maintain the high fidelity of DNA replication and transcription under oxidative stress [44,45]. In addition, Mut-T in *E. coli* hydrolyzes 8-oxo-GTP to 8-oxo-GMP which cannot be used by the cells for RNA synthesis, thus sanitizing the cellular pools of the oxidized nucleotides [46]. Equivalent function in humans is performed by MTH1 [47].

In the present study, we characterize the transcriptional fidelity of RpoTm from *Arabidopsis thaliana* during the elongation phase on a complete DNA scaffold. In addition, we probe the propensity of RpoTm to misincorporate normal as well as oxidized NTPs into RNA and for translesion bypass on oxidatively damaged DNA template. Among oxidized ribonucleotides tested, 8-oxo-GTP and 2-hydroxy-ATP both get incorporated into growing RNA by RpoTm opposite to adenine, cytosine, and thymine. Steady-state kinetics reveals that the misincorporation of 8-oxo-GTP and 2-hydroxy-ATP into RNA ensues with higher K_m and lower catalytic efficiency compared to the correct base. This is in contrast to what has been observed earlier for multisubunit RNAP from *E. coli* [12]. The oxidized bases are incorporated with similar efficiency as the mismatches by RpoTm into the growing RNA. Similarly, the catalytic efficiency of 8-oxo-GTP incorporation by T7 RNAP was calculated to be lower than that of guanine incorporation opposite to dC, indicating that this may be a general feature of the single-subunit RNAP. In addition, the experiments reveal that abasic site or 8-oxo-adenine DNA

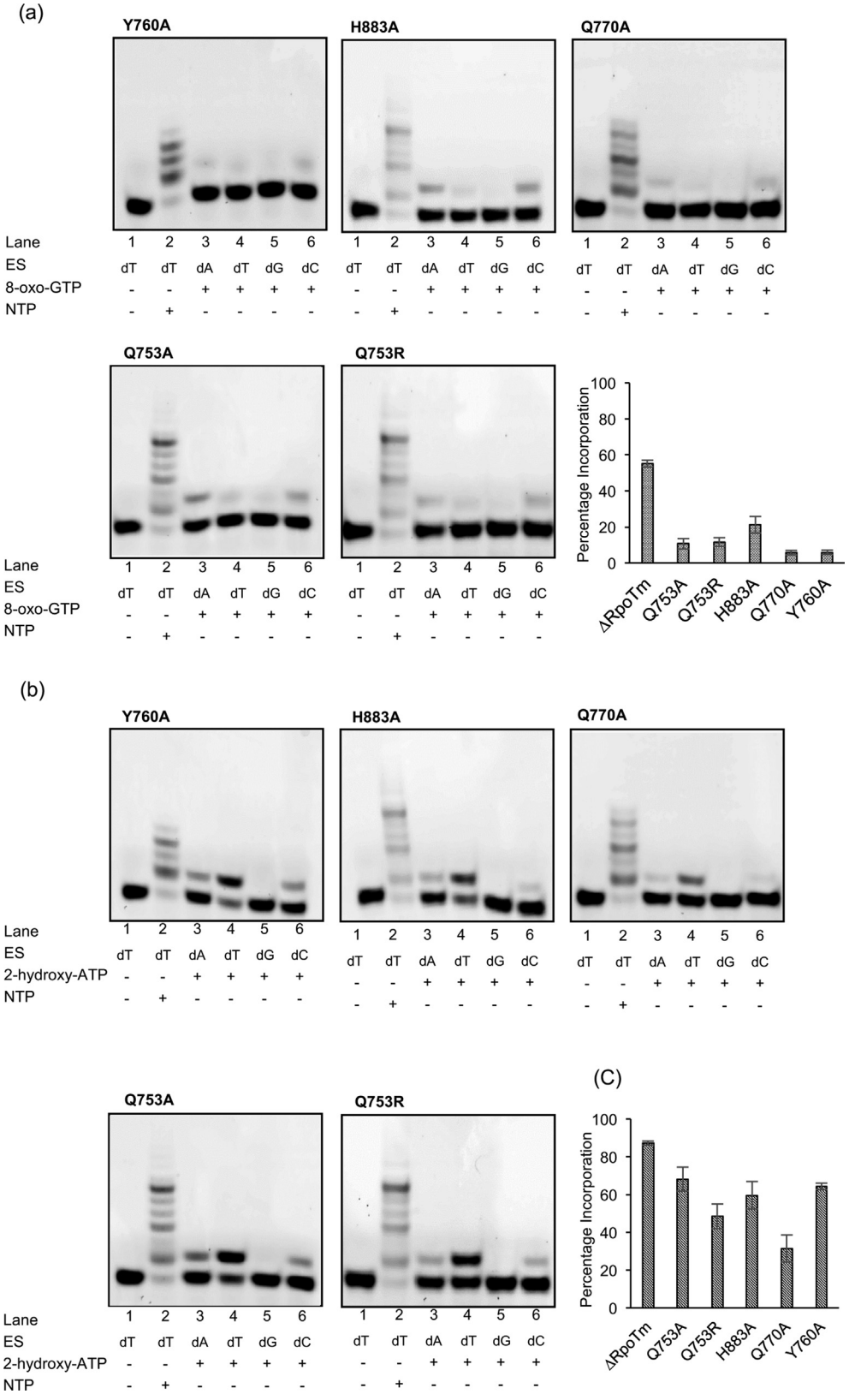
(a)
Y760A
H883A
Q770A
Q753A
Q753R
Lane 1 2 3 4 5 6
ES dT dT dA dT dG dC
8-oxo-GTP - - + + + +
NTP - + - - - -
Percentage Incorporation
100
80
60
40
20
0
ΔRpoTm
Q753A
Q753R
H883A
Q770A
Y760A
(b)
2-hydroxy-ATP
(C)

lesions cause a block of transcription, while 8-oxo-guanine DNA lesion is mutagenic because extension beyond 8-oxo-guanine was observed.

Single-polypeptide RNAPs have neither backtracking activity nor auxiliary proofreading-enhancing protein factors [25,48,49]. Moreover, the absence of a MuT-T type hydrolase and nonexisting BER pathway in mitochondria of plants suggests that plants may have evolved unique strategies against the oxidized nucleotides. Through our study, we demonstrate that RpoTm uses three mechanisms to combat the oxidative environment of mitochondria: (i) stringent selection against misincorporation of the noncognate nucleotides as compared with unmodified nucleotides, (ii) inefficient incorporation of the oxidized nucleotides, and (iii) stalling of transcription upon encountering lesions such as abasic site and 8-oxo-dA in the DNA. Thus, the fidelity of RpoTm is entirely relying on its ability to discriminate between the correct and incorrect nucleotide in the absence of postincorporation proofreading. These properties are in contrast to what was observed for multisubunit RNAP of *E. coli* where 8-oxo-GTP incorporation opposite to dA and dC was found to be more efficient as compared with unoxidized guanine.

Transcriptional error rates range from 10^{-4} to 10^{-5}, which are much higher than those in DNA replication (10^{-9} per residue). Although higher fidelity is desirable for the faithful transfer of genetic information, the transcriptional errors are transient and have received much less attention. The errors during replication are the basis of evolution and are transmitted to subsequent generation and hence the DNA polymerases have evolved to be high-fidelity enzymes. Transcriptional errors on the other hand are more endured. Estimates of the error rates of single-subunit enzymes show that their fidelity is closer to DNAPs in the absence of proof reading activity. The fidelity of the polymerase is dictated by the active site conformations which differ significantly between the multisubunit and single-subunit RNAPs.

However, the catalytic mechanism between different RNAP is highly conserved. In addition, the various factors such as Gre and TFIIS modulate the error rates of multi-subunit enzymes. Hence, the efficiency of incorporation and the error rates are significantly different. Evolutionarily, the multisubunit enzymes are unrelated to the single-subunit RNAPs. The single-subunit RNAPs share their architecture with phage and DNA polymerases and are believed to be evolved from them [50]. Thus, the stringency of selection of the substrate and hence the fidelity of base incorporation by single-subunit RNAPs resembles that of DNA polymerases when compared in the absence of proof reading activity of the latter.

Materials and Methods

Cloning of full-length RpoTm

For cloning RpoTm (locus tag At1g68990), RNA was extracted from the leaves of *Arabidopsis thaliana* (concentration: 1 μg/μl). High-capacity RNA-to-cDNA Kit (Applied Biosystems) was used for cDNA synthesis. From the cDNA, RpoTm (locus tag At1g68990) (from amino acid 43 to 946 without the mitochondrial targeting peptide) was fished out and cloned into *Eco*RI and *Not*I sites into a modified pET21b plasmid. The gene segment of RpoTm was fused to an upstream hexa-histidine tag with a PreScission-cleavable linker (pDJN1) to yield plasmid pDJN1 RpoTm. ΔRpoTm (58–976 amino acids) was cloned using the full-length clone as the template.

Site-directed mutagenesis

RpoTm D909A mutant protein was prepared by Quick Change site-directed mutagenesis kit (Agilent technologies) using full-length RpoTm as the template. For the Q770A, Q753A, Q753R, H883A, and Y760A mutants ΔRpoTm was used as a template. Clones obtained were confirmed by sequencing for the presence of the mutation.

Overexpression and purification

RpoTm plasmid was transformed into codon plus cells and grown at 37 °C in LB till OD_{600} reached to 0.6–0.8. Overexpression of the protein was induced by addition of 0.1 mM of IPTG at 18 °C for 18 h. Cells were harvested and resuspended in lysis buffer (25 mM Tris pH-7.5, 500 mM NaCl, 5% glycerol, 2 mM β-mercaptoethanol, and 1 mM PMSF). Cells were sonicated and centrifuged at 16,000 rpm for 45 min. The supernatant was filtered and used for His-trap affinity chromatography with a step gradient (imidazole concentration) elution. The eluent from His-trap affinity chromatography was subjected to PreScission protease for cleavage of the tag. Heparin chromatography and size exclusion chromatography (HiTrap™ Heparin HP and Superdex 200 GE) were performed after digestion. Protein was finally eluted in gel filtration buffer (25 mM Tris pH 7.5, 250 mM NaCl, 5%

Fig. 8. The transcriptional efficiency of mutant ΔRpoTm: (a) The gel pictures showing extension of 150 nM of scaffolds incubated with 2 μM of no NTP (lane 1), 8-oxo-GTP (lane 3, 4, 5, and 6), and NTP mix (lane 2 and 8). Reactions in different gels were initiated by adding various ΔRpoTm mutants at 300 nM. The mutant for each gel is depicted on the top. (b) The gel pictures showing extension of 150 nM of different DNA:RNA scaffolds incubated with 2 μM of no NTP (lane 1), 2-hydroxy-ATP (lane 3, 4, 5, and 6), and NTP mix (lane 2). Reactions in different gels were initiated by adding various ΔRpoTm mutants at 300 nM. The mutant for each gel is depicted on the top (c) Plot showing percentage incorporation of 2-hydroxy-ATP by wtΔRpoTm and various mutants.

glycerol, and 2 mM DTT). The purity of the protein was assessed by sodium dodecyl sulfate–polyacrylamide gel electrophoresis and the final concentration was estimated using the bicinchoninic acid (BCA) protein assay (Thermo Scientific). The protein was also subjected to mass spectrometry to assess its purity and confirm the molecular weight. ΔRPoTm mutants (Q770A, Q753A, Q753R, H883A, and Y760A) were purified using the affinity chromatography as performed for the wild-type enzyme.

Oligonucleotide annealing

The oligonucleotides were custom synthesized and HPLC purified by Eurofins Genomics. The oligonucleotides containing DNA lesion were custom synthesized and HPLC purified from Sigma-Aldrich. The template (38nt), nontemplate DNA (38nt) strands were mixed with 5′6-FAM–labeled RNA (8nt) in the ratio 1.25:1.5:1 and annealed by heating at 90 °C for 5 min followed by cooling at room temperature. For DNA containing the lesion, the DNA and RNA strands were mixed in the ratio 1.2:1 and annealed as previously described.

Fluorescence anisotropy

6-FAM–labeled ES8T (5 nM) was titrated with increasing concentration of ΔRpoTm in the buffer containing 25 mM Tris pH, 7.5, 100 mM NaCl, and 2 mM DTT at 25 °C. Fluorescence anisotropy readings (SpectraMax M5 plate reader, Molecular Devices) were recorded at 492 nm (excitation) and 517 nm (emission) and plotted against the ΔRpoTm concentration. The data were then fitted to the specific binding with the Hill slope equation to obtain the equilibrium dissociation constant (K_d) in GraphPad Prism 7. The off-rates (k_{off}) of ES:RpoTm complex were determined by chasing a complex of FAM-labeled ES8T (5 nM) and ΔRpoTm (60 nM) with unlabeled ES8 (500nM) and the dissociation of FAM-labeled ES8 from the ΔRpoTm was observed by monitoring the decrease in fluorescence anisotropy. The data were fitted to one phase decay equation (GraphPad Prism 7) to obtain the off-rates (k_{off}).

Transcription assay

150 nM of the ES8 was taken in the 1X reaction buffer containing 25 mM Tris pH 7.5, 15 mM $MgCl_2$, 1 mM DTT, and 0.05 mg/ml BSA in a total of 10 μl reaction volume and mixed with 2 μM NTP or the modified bases such as 8-oxo-GTP or 2-hydroxy-ATP. The reaction was initiated using RpoTm at 300 nM and incubated at 27 °C for 30 min. Reaction was stopped using 5 μl of stop solution containing 20 mM EDTA, 80% formamide, 1 mg/ml xylene cyanol, and 1 mg/ml bromophenol blue. The samples were heated for 5 min at 95 °C before loading on a 24% PAGE containing 8 M urea and run in the 1X TBE buffer. Resolved products were then observed by excitation at 488 nm and the bands were visualized and recorded using a Typhoon FLA 7000 scanner (GE Healthcare). The intensity of the observed bands was quantified using Image Quant TL, 1D gel analysis software. T7 RNAP was procured from NEB (Catalog number M0251S) and the assay was performed as previously described using 300 nM of enzyme and 50 μM of NTPs.

For lesion bypass, synthetic DNA oligonucleotides containing lesions (8-oxo-guanine, AP site, 8-oxo-adenine) (Sigma) at the ninth position from the 3′ position were hybridized with the corresponding 8-mer FAM-labeled RNA. The assay is performed by taking 150 nM of scaffold, 50 μM NTP, and 300 nM ΔRpoTm at 27 °C. Any deviation in the reaction condition is mentioned in the corresponding figure legend.

Steady-state kinetics

Initially time course reactions were carried out to establish a time point at which not more than 20% of the primer had been extended [45]. These reactions were carried out for the template base–incoming nucleotide combinations. Two hundred nM of the scaffold was mixed with varying concentrations of the incoming NTP and 15 nM of RpoTm (except for some miss incorporation kinetics). The reaction was carried out at 27 °C for 10 min. In case of (1) dA:ATP, dC:2-hydroxy-ATP; (2) dG:GTP, dA:2-hydroxy-ATP; and (3) dT:8-oxo-GTP misincorporations, the enzyme concentration taken was 60 nM, 80 nM, and 100 nM, respectively, and the reaction was carried out at 27 °C for 15 min. For Q753A ΔRpoTm, the kinetics of dT:ATP and dT:2-hydroxy-ATP was carried out at 20 nM and 50 nM of enzyme, respectively. The products were then resolved on a 24% polyacrylamide gel containing 8 M urea. The resolved products were observed by excitation at 488 nm, and the bands were visualized and recorded using a Typhoon FLA 7000 scanner (GE Healthcare). The intensity of the observed bands was quantified using Image Quant TL, 1D gel analysis software. Steady-state kinetic parameters, K_m and V_{max} for each combination of template and incoming nucleotide were determined using a Lineweaver-Burk plot.

Homology modeling of RpoTm

A homology model of RpoTm was constructed based on the elongation complex structure of T7 RNAP (PDB ID: 1S76). The model includes the RNA primer, DNA template, and two bound Mg^{2+} ions. The modeling was carried out using Discovery Studio 3.5 (Dassault Systèmes BIOVIA, Discovery Studio Modelling Environment). Subsequently, the nonhydrolyzable ATP (i.e., APC) was modified to GTP, ATP, 8-oxo-GTP, and 2-OH ATP, and the templating base dT was mutated to dA and dC in Coot [51]. The sequence of the 1S76 structure was aligned against the target sequence to identify the matched regions. Based on the atomic coordinates of the T7 RNAP structure, the ΔRpoTm structure was modeled. After modification, the final model was energy minimized using the steepest descent (steps 200) with the CHARMM (Chemistry at HARvard Molecular Mechanics) force field. During energy minimization, the DNA-RNA complex was constrained to reduce distortion in the DNA-RNA backbone. Constructed models were verified by Ramachandran plot in Coot and the figure was generated in PyMol. For further analysis, the CONTACT program of CCP4 [52] was used to find the interacting amino acid residues with incoming NTP within the 4 Å radius.

Acknowledgments

The authors thank Dr. P.V. Shivaprasad, NCBS, Bangalore, for whole leaf RNA from *Arabidopsis thaliana.* The work was supported by Early Career Research grant (ECR/2015/000042 to DJ) from the Science and Engineering Research Board - Department of Science and Technology (Government of India) and intramural funds available from the Regional Centre for Biotechnology. A.K.Y. is supported by the Young Investigator Program of RCB. P.K.S. is supported by the fellowship from the Council of Scientific and Industrial Research.

Appendix A. Supplementary data

Supplementary data to this article can be found online at https://doi.org/10.1016/j.jmb.2019.08.022.

Received 17 September 2018;
Received in revised form 30 May 2019;
Accepted 26 August 2019
Available online 15 October 2019

Keywords:
Mitochondrial RNAP;
Transcription;
8-Oxo-guanine;
Arabidopsis thaliana;
ROS

†Equal contribution.

References

[1] P. Gamba, N. Zenkin, Transcription fidelity and its roles in the cell, Curr. Opin. Microbiol. 42 (2018) 13–18, https://doi.org/10.1016/J.MIB.2017.08.004.

[2] L.B. Carey, RNA polymerase errors cause splicing defects and can be regulated by differential expression of RNA polymerase subunits, Elife 4 (2015), https://doi.org/10.7554/eLife.09945.

[3] M. Vermulst, A.S. Denney, M.J. Lang, C.-W. Hung, S. Moore, A.M. Mosely, W.J. Thompson, V. Madden, J. Gauer, K.J. Wolfe, D.W. Summers, J. Schleit, G.L. Sutphin, S. Haroon, A. Holczbauer, J. Caine, J. Jorgenson, D. Cyr, M. Kaeberlein, J.N. Strathern, M.C. Duncan, D.A. Erie, Transcription errors induce proteotoxic stress and shorten cellular lifespan, Nat. Commun. 6 (2015) 8065, https://doi.org/10.1038/ncomms9065.

[4] A.J.E. Gordon, D. Satory, J.A. Halliday, C. Herman, Heritable change caused by transient transcription errors, PLoS Genet. 9 (2013), e1003595, https://doi.org/10.1371/journal.pgen.1003595.

[5] J.F. Morreall, L. Petrova, P.W. Doetsch, Transcriptional mutagenesis and its potential roles in the etiology of cancer and bacterial antibiotic resistance, J. Cell. Physiol. 228 (2013) 2257–2261, https://doi.org/10.1002/jcp.24400.

[6] D.A. Erie, O. Hajiseyedjavadi, M.C. Young, P.H. von Hippel, Multiple RNA polymerase conformations and GreA: control of the fidelity of transcription, Science 262 (1993) 867–873. http://www.ncbi.nlm.nih.gov/pubmed/8235608. (Accessed 7 June 2018).

[7] M.J. Thomas, A.A. Platas, D.K. Hawley, Transcriptional fidelity and proofreading by RNA polymerase II, Cell 93 (1998) 627–637. http://www.ncbi.nlm.nih.gov/pubmed/9604937. (Accessed 8 June 2018).

[8] A. Nunomura, P.I. Moreira, R.J. Castellani, H.G. Lee, X. Zhu, M.A. Smith, G. Perry, Oxidative damage to RNA in aging and neurodegenerative disorders, Neurotox. Res. 22 (2012) 231–248, https://doi.org/10.1007/s12640-012-9331-x.

[9] E.K. Hudson, B.A. Hogue, N.C. Souza-Pinto, D.L. Croteau, R.M. Anson, V.A. Bohr, R.G. Hansford, Age-associated change in mitochondrial DNA damage, Free Radic. Res. 29 (1998) 573–579. https://www.ncbi.nlm.nih.gov/pubmed/10098461.

[10] M. Tanaka, P.B. Chock, E.R. Stadtman, Oxidized messenger RNA induces translation errors, Proc. Natl. Acad. Sci. U. S. A. 104 (2007) 66–71, https://doi.org/10.1073/pnas.0609737104.

[11] Y.H. Chen, D.F. Bogenhagen, Effects of DNA lesions on transcription elongation by T7 RNA polymerase, J. Biol. Chem. 268 (1993) 5849–5855. https://www.ncbi.nlm.nih.gov/pubmed/8449951.

[12] H. Kamiya, A. Suzuki, Y. Yamaguchi, H. Handa, H. Harashima, Incorporation of 8-hydroxyguanosine (8-oxo-7,8-dihydroguanosine) 5′-triphosphate by bacterial and human RNA polymerases, Free Radic. Biol. Med. 46 (2009) 1703–1707, https://doi.org/10.1016/j.freeradbiomed.2009.04.005.

[13] P.W. Doetsch, Translesion synthesis by RNA polymerases: occurrence and biological implications for transcriptional mutagenesis, Mutat. Res. Mol. Mech. Mutagen. 510 (2002) 131–140, https://doi.org/10.1016/S0027-5107(02)00258-0.

[14] I. Kuraoka, M. Endou, Y. Yamaguchi, T. Wada, H. Handa, K. Tanaka, Effects of endogenous DNA base lesions on transcription elongation by mammalian RNA polymerase II. Implications for transcription-coupled DNA repair and transcriptional mutagenesis, J. Biol. Chem. 278 (2003) 7294–7299, https://doi.org/10.1074/jbc.M208102200.

[15] G.E. Damsma, A. Alt, F. Brueckner, T. Carell, P. Cramer, Mechanism of transcriptional stalling at cisplatin-damaged DNA, Nat. Struct. Mol. Biol. 14 (2007) 1127–1133, https://doi.org/10.1038/nsmb1314.

[16] B. Hedtke, T. Borner, A. Weihe, Mitochondrial and chloroplast phage-type RNA polymerases in Arabidopsis, Science (80–) 277 (1997) 809–811. https://www.ncbi.nlm.nih.gov/pubmed/9242608.

[17] H.P. Braun, S. Binder, A. Brennicke, H. Eubel, A.R. Fernie, I. Finkemeier, J. Klodmann, A.C. Konig, K. Kuhn, E. Meyer, T. Obata, M. Schwarzlander, M. Takenaka, A. Zehrmann, The life of plant mitochondrial complex I, Mitochondrion 19 Pt B (2014) 295–313, https://doi.org/10.1016/j.mito.2014.02.006.

[18] K. Kuhn, U. Richter, E.H. Meyer, E. Delannoy, A.F. de Longevialle, N. O'Toole, T. Borner, A.H. Millar, I.D. Small, J. Whelan, Phage-type RNA polymerase RPOTmp performs gene-specific transcription in mitochondria of Arabidopsis thaliana, Plant Cell 21 (2009) 2762–2779, https://doi.org/10.1105/tpc.109.068536.

[19] D. Temiakov, V. Patlan, M. Anikin, W.T. McAllister, S. Yokoyama, D.G. Vassylyev, Structural basis for substrate

selection by t7 RNA polymerase, Cell 116 (2004) 381–391. http://www.ncbi.nlm.nih.gov/pubmed/15016373. (Accessed 2 June 2018).
[20] D.W.A. Buchan, F. Minneci, T.C.O. Nugent, K. Bryson, D.T. Jones, Scalable web services for the PSIPRED protein analysis workbench, Nucleic Acids Res. 41 (2013) W349–W357, https://doi.org/10.1093/nar/gkt381.
[21] C.D.O. Cooper, B.D. Marsden, N- and C-terminal truncations to enhance protein solubility and crystallization: predicting protein domain boundaries with bioinformatics tools, 2017, pp. 11–31, https://doi.org/10.1007/978-1-4939-6887-9_2.
[22] T.A. Kunkel, DNA replication fidelity, J. Biol. Chem. 279 (2004) 16895–16898, https://doi.org/10.1074/jbc.R400006200.
[23] S. Sultana, M. Solotchi, A. Ramachandran, S.S. Patel, Transcriptional fidelities of human mitochondrial POLRMT, yeast mitochondrial Rpo41, and phage T7 single-subunit RNA polymerases, J. Biol. Chem. 292 (2017) 18145–18160, https://doi.org/10.1074/jbc.M117.797480.
[24] F. Faucher, S. Doublie, Z. Jia, 8-oxoguanine DNA glycosylases: one lesion, three subfamilies, Int. J. Mol. Sci. 13 (2012) 6711–6729, https://doi.org/10.3390/ijms13066711.
[25] J. Huang, L.G. Brieba, R. Sousa, Misincorporation by wild-type and mutant T7 RNA polymerases: identification of interactions that reduce misincorporation rates by stabilizing the catalytically incompetent open conformation †, Biochemistry 39 (2000) 11571–11580, https://doi.org/10.1021/bi000579d.
[26] R.A. Ganai, E. Johansson, Molecular Cell DNA Replication-A Matter of Fidelity, 2016, https://doi.org/10.1016/j.molcel.2016.05.003.
[27] B.S. Strauss, The "A" rule revisited: polymerases as determinants of mutational specificity, DNA Repair (Amst) 1 (2002) 125–135, https://doi.org/10.1016/S1568-7864(01)00014-3.
[28] S. Tornaletti, L.S. Maeda, R.D. Kolodner, P.C. Hanawalt, Effect of 8-oxoguanine on transcription elongation by T7 RNA polymerase and mammalian RNA polymerase II, DNA Repair (Amst) 3 (2004) 483–494, https://doi.org/10.1016/J.DNAREP.2004.01.003.
[29] A. Viswanathan, P.W. Doetsch, Effects of nonbulky DNA base damages on Escherichia coli RNA polymerase-mediated elongation and promoter clearance, J. Biol. Chem. 273 (1998) 21276–21281. https://www.ncbi.nlm.nih.gov/pubmed/9694887.
[30] D. Bregeon, P.A. Peignon, A. Sarasin, Transcriptional mutagenesis induced by 8-oxoguanine in mammalian cells, PLoS Genet. 5 (2009), e1000577, https://doi.org/10.1371/journal.pgen.1000577.
[31] G.E. Damsma, P. Cramer, Molecular basis of transcriptional mutagenesis at 8-oxoguanine, J. Biol. Chem. 284 (2009) 31658–31663, https://doi.org/10.1074/jbc.M109.022764.
[32] K. Schwinghammer, A.C. Cheung, Y.I. Morozov, K. Agaronyan, D. Temiakov, P. Cramer, Structure of human mitochondrial RNA polymerase elongation complex, Nat. Struct. Mol. Biol. 20 (2013) 1298–1303, https://doi.org/10.1038/nsmb.2683.
[33] Y.W. Yin, T.A. Steitz, The structural mechanism of translocation and helicase activity in T7 RNA polymerase, Cell 116 (2004) 393–404. https://www.ncbi.nlm.nih.gov/pubmed/15016374.
[34] T.A. Steitz, The structural changes of T7 RNA polymerase from transcription initiation to elongation, Curr. Opin. Struct. Biol. 19 (2009) 683–690, https://doi.org/10.1016/j.sbi.2009.09.001.
[35] R. Sousa, R. Padilla, A mutant T7 RNA polymerase as a DNA polymerase, EMBO J. 14 (1995) 4609–4621. https://www.ncbi.nlm.nih.gov/pubmed/7556104.
[36] J. Huang, R. Sousa, T7 RNA polymerase elongation complex structure and movement, J. Mol. Biol. 303 (2000) 347–358, https://doi.org/10.1006/jmbi.2000.4150.
[37] G. Bonner, D. Patra, E.M. Lafer, R. Sousa, Mutations in T7 RNA polymerase that support the proposal for a common polymerase active site structure, EMBO J. 11 (1992) 3767–3775. https://www.ncbi.nlm.nih.gov/pubmed/1396570.
[38] G. Bonner, E.M. Lafer, R. Sousa, Characterization of a set of T7 RNA polymerase active site mutants, J. Biol. Chem. 269 (1994) 25120–25128. http://www.ncbi.nlm.nih.gov/pubmed/7929200. (Accessed 7 June 2018).
[39] V.L. Tunitskaya, S.N. Kochetkov, Structural-functional analysis of bacteriophage T7 RNA polymerase, Biochemistry (Mosc.) 67 (2002) 1124–1135. http://www.ncbi.nlm.nih.gov/pubmed/12460110. (Accessed 7 June 2018).
[40] C.K. Surratt, S.C. Milan, M.J. Chamberlin, Spontaneous cleavage of RNA in ternary complexes of Escherichia coli RNA polymerase and its significance for the mechanism of transcription, Proc. Natl. Acad. Sci. U. S. A. 88 (1991) 7983–7987. https://www.ncbi.nlm.nih.gov/pubmed/1716768.
[41] H. Koyama, T. Ito, T. Nakanishi, N. Kawamura, K. Sekimizu, Transcription elongation factor S-II maintains transcriptional fidelity and confers oxidative stress resistance, Genes Cells 8 (2003) 779–788. https://www.ncbi.nlm.nih.gov/pubmed/14531857.
[42] H. Hayakawa, T. Uchiumi, T. Fukuda, M. Ashizuka, K. Kohno, M. Kuwano, M. Sekiguchi, Binding capacity of human YB-1 protein for RNA containing 8-oxoguanine, Biochemistry 41 (2002) 12739–12744. https://www.ncbi.nlm.nih.gov/pubmed/12379116.
[43] A.B. Britt, DNA damage and repair in plants, Annu. Rev. Plant Physiol. Plant Mol. Biol. 47 (1996) 75–100, https://doi.org/10.1146/annurev.arplant.47.1.75.
[44] S. Boiteux, J.P. Radicella, Base excision repair of 8-hydroxyguanine protects DNA from endogenous oxidative stress, Biochimie 81 (1999) 59–67. https://www.ncbi.nlm.nih.gov/pubmed/10214911.
[45] M.S. Boosalis, J. Petruska, M.F. Goodman, DNA polymerase insertion fidelity. Gel assay for site-specific kinetics, J. Biol. Chem. 262 (1987) 14689–14696. https://www.ncbi.nlm.nih.gov/pubmed/3667598.
[46] F. Taddei, H. Hayakawa, M. Bouton, A. Cirinesi, I. Matic, M. Sekiguchi, M. Radman, Counteraction by MutT protein of transcriptional errors caused by oxidative damage, Science (80–) 278 (1997) 128–130. https://www.ncbi.nlm.nih.gov/pubmed/9311918.
[47] T. Ishibashi, H. Hayakawa, R. Ito, M. Miyazawa, Y. Yamagata, M. Sekiguchi, Mammalian enzymes for preventing transcriptional errors caused by oxidative damage, Nucleic Acids Res. 33 (2005) 3779–3784, https://doi.org/10.1093/nar/gki682.
[48] Y.W. Yin, T.A. Steitz, The structural mechanism of translocation and helicase activity in T7 RNA polymerase, Cell 116 (2004) 393–404, https://doi.org/10.1016/S0092-8674(04)00120-5.
[49] L.-T. Da, C. E, Y. Shuai, S. Wu, X.-D. Su, J. Yu, T7 RNA polymerase translocation is facilitated by a helix opening on the fingers domain that may also prevent backtracking, Nucleic Acids Res. 45 (2017) 7909–7921, https://doi.org/10.1093/nar/gkx495.

[50] N. Cermakian, T.M. Ikeda, P. Miramontes, B.F. Lang, M.W. Gray, R. Cedergren, On the evolution of the single-subunit RNA polymerases, J. Mol. Evol. 45 (1997) 671–681. http://www.ncbi.nlm.nih.gov/pubmed/9419244. (Accessed 12 December 2017).

[51] P. Emsley, B. Lohkamp, W.G. Scott, K. Cowtan, Features and development of Coot, Acta Crystallogr. Sect. D Biol. Crystallogr. 66 (2010) 486–501, https://doi.org/10.1107/S0907444910007493.

[52] M.D. Winn, C.C. Ballard, K.D. Cowtan, E.J. Dodson, P. Emsley, P.R. Evans, R.M. Keegan, E.B. Krissinel, A.G.W. Leslie, A. McCoy, S.J. McNicholas, G.N. Murshudov, N.S. Pannu, E.A. Potterton, H.R. Powell, R.J. Read, A. Vagin, K.S. Wilson, Overview of the CCP 4 suite and current developments, Acta Crystallogr. Sect. D Biol. Crystallogr. 67 (2011) 235–242, https://doi.org/10.1107/S0907444910045749.

[53] R. Ringel, M. Sologub, Y.I. Morozov, D. Litonin, P. Cramer, D. Temiakov, Structure of human mitochondrial RNA polymerase, Nature 478 (2011) 269–273, https://doi.org/10.1038/nature10435.